applied sciences

MDPI

Article

Robust Design of Deep Drawing Process through In-Line Feedback Control of the Draw-In

Luigi Tricarico and Maria Emanuela Palmieri *

Department of Mechanical Engineering, Mathematics & Management Engineering, Politecnico of Bari, 70126 Bari, Italy
* Correspondence: mariaemanuela.palmieri@poliba.it

Abstract: In the deep drawing process, the scatter of the friction coefficient between blank and tool interfaces as well as of the material properties between blank positions in the coil or between different coils significantly influences the part quality. These uncontrollable fluctuations increase the risk of waste. To avoid this problem, currently, the new era of Industry 4.0 aims at developing control algorithms able to in-line adjust process parameters and always meet the part quality requirements. Starting from this context, in this study a method for process control during the punch stroke is proposed. It assumes the blank draw-in in specific points as the control variable, while the blank holder force is adopted as an in-line adjustable process parameter. The approach was implemented for the deep drawing of a T-shaped component, using a blank in DC05 steel with a thickness of 0.75 mm. The results show that the measurement of blank draw-in is a representative index of the component quality, which in this study is evaluated in terms of formability (thinning) and cosmetic (surface deflections) defects. Once the optimal condition and the corresponding blank draw-in were identified, the feedback control algorithm was able to increase or reduce the blank holder force according to whether the recorded draw-in was higher or lower than the optimal one.

Keywords: deep drawing; feedback closed-loop control; draw-in; laser triangulation sensors; blank holder force

Citation: Tricarico, L.; Palmieri, M.E. Robust Design of Deep Drawing Process through In-Line Feedback Control of the Draw-In. *Appl. Sci.* **2023**, *13*, 1717. https://doi.org/10.3390/app13031717

Academic Editors: Michael Oluwatosin Bodunrin, Desmond Klenam and Japheth Obiko

Received: 25 December 2022
Revised: 24 January 2023
Accepted: 27 January 2023
Published: 29 January 2023

1. Introduction

The deep drawing process, thanks to its high productivity, is a sheet metal forming process commonly adopted in the automotive, aeronautical, and food industries [1–4]. In this process, the blank is forced by a punch inside a die while it is held down against the die by a blank holder which applies a force [2]. The blank holder force is one of the most influential process parameters [5–9]. Specifically, the increase in the blank holder force leads to a reduction in material sliding, causing the risk of splits. Conversely, a reduction in the blank holder force leads to the material sliding in the die, causing the risk of wrinkles [10]. The blank holder force is a process parameter, which is usually optimized to obtain a defect-free component. However, while aiming for zero-defect production through a careful design, noise factors can affect the final quality of the deep-drawn component. The main influences in series production are: (a) Material fluctuations along the same coil or between different coils [11]. (b) The variation in the lubrication conditions due, for example, to the increase in tool temperature during the process and/or to the presence of residual lubricant on the tool surface and/or to inaccurate and inhomogeneous lubricant distribution on the blank surface [12]. These fluctuations could lead to a scrapped deep-drawn component. For this reason, several studies [13–15] carried out a robustness analysis with the aim of identifying a wide operating window in which to obtain components without defects. However, due to the complexity of the components, especially in the automotive industry, wide operating windows are difficult to obtain. To overcome this problem, current research is moving in two directions, i.e., forward-type control and closed-loop feedback-type control.

The feed-forward control is a predictive type of control, which consists in measuring the coil material properties or the lubricant thickness on the blank before the process in order to control the noise variables and identify the optimal process parameters to set during the process. Palmieri et al. [8] performed a numerical study for the identification of regulation curves of the blank holder force as a function of the friction coefficient and the yield strength of the material to be measured on the blank entering the press machine. Research carried out by Fischer et al. [12,16–18] on the deep drawing of a kitchen sink involved the use of an eddy current sensor to measure the material's yield strength, tensile strength, uniform elongation, elongation at break, and initial material grain size. These material data were used as the input parameter for the finite element simulations, whose results were adopted to generate the metamodels useful to determine the process window. Therefore, these data were used as input for the feed-forward control during the process. For a feed-forward-type control, several non-destructive measurement methods (eddy current instruments, laser triangulation sensor equipment, 3MA instrument-Fraunhofer IZFP) were developed, although they still need further development for industrial production applications [19].

The closed-loop feedback-type control, on the other hand, operates with the aim of adjusting in-line the process parameter that can be controlled by means of actuators in order to identify a new operating point under new working conditions. For this kind of control, it is necessary to identify both a sensor capable of measuring the feedback value representative of the noise and an actuator capable of regulating the controllable process parameter. Several studies considered the blank draw-in as the main indicator of quality and therefore as the feedback value to be measured during the process. The blank holder force, instead, was adopted as a controllable process parameter to be adjusted [9,20–22].

For many years, scientific studies investigated sensor systems for the measurement of the draw-in amount. Lo et al. [23] adopted a reflective photoelectric encoder; Doege et al. [24] developed a computer-mouse-like ball sensor based on the mechanical transmission of the plane movement of the blank onto a ball; Doege et al. [25] also designed a contactless optical sensor which consists of a chip with a complementary metal oxide semiconductor (CMOS) sensor and a digital signal processor (DSP); and other authors studied inductance sensors [26]. Laser triangulation sensors are generally the most adopted ones since they can capture in-line the entire draw-in profile by means of an optical non-contact measurement [27]. Moreover, the latest generation laser triangulation sensors are characterized by a high frequency response, making them ideal for in-line process monitoring.

The blank holder, on the other hand, itself acts as an actuator. Due to the complexity of components, a huge number of sensors and actuators acting locally can be required. Consequently, in some studies [28,29] piezoelectric actuators were implemented inside the die with the aim of locally modifying the material sliding. Moreover, other research [30] studied magnetorheological fluid-based devices embedded within the blank holder to adjust the pressure by using a closed-control approach.

In this work, a closed-loop feedback-type control was studied to manufacture, by means of a deep drawing process, a defect-free component even in the presence of noise factors. The blank holder force was adjusted by means of a proportional–derivative–integrative controller, measuring the blank draw-in. This control was successfully implemented with a numerical method after calibration of the finite element model by means of experimental tests.

To avoid the use of several sensors and locally acting actuators, the innovation in the methodology proposed here consists in the feedback control based on the draw-in value recorded by the only sensor which is more sensitive to the fluctuations of the uncontrollable parameters.

2. Materials and Methods

This study presents a methodology aimed at minimizing the influence of scattering in material properties and in lubrication conditions during a deep drawing process to achieve a zero-failure product. The adopted approach proposes the in-line optical measurement of the blank draw-in and the in-line adjustment of the blank holder force.

The methodology is described for the T-shaped component shown in Figure 1, chosen as the case study. The part shape was purposely chosen to analyze typical defects of the drawing process, such as formability and cosmetic defects. First, a finite element (FE) model in AutoForm-Sigma R10® was developed for the deep drawing simulation of the part, and preliminary experimental tests were performed to calibrate the numerical model. These tests were carried out on the 3000 kN hydraulic press machine designed and manufacturing by GIGANT Italia in collaboration with industrial and academic partners of the PICO&PRO project. A passive blank holder moved by a hydraulic actuator with a maximum hydraulic force of 1000 kN and a response time of 100 ms was adopted in this press.

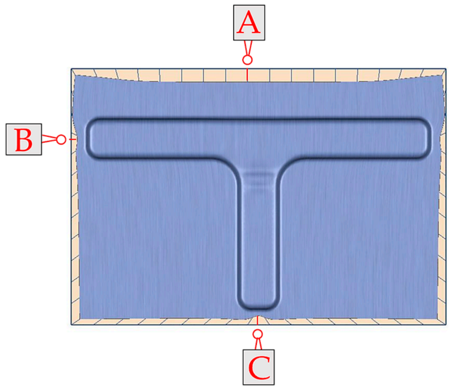

Figure 1. T-shaped component and points where the drw-in was monitored (A, B and C).

The calibration of the numerical model was carried out by detecting the friction coefficient value so that FE draw-in matched the experimental one. The draw-in was evaluated at the points highlighted with the letters A, B, and C in Figure 1. Laser triangulation sensors (LK-G5000 Keyence, Osaka, Japan) were adopted near these points for experimentally acquiring the draw-in (Figure 2). These sensors had a sampling speed of 392 kHz, an accuracy of ±0.02%, and a repeatability of 0.01 μm, hence were able to perform accurate measurements during the in-line process. A 100 Mbps Ethernet communication interface was finally chosen to connect the sensors to a programmable logic controller (PLC), Siemens S7-1500 (Siemens, Munich, Germany) with CPU 1515T-2 PN, for controlling the measurements of the draw-in.

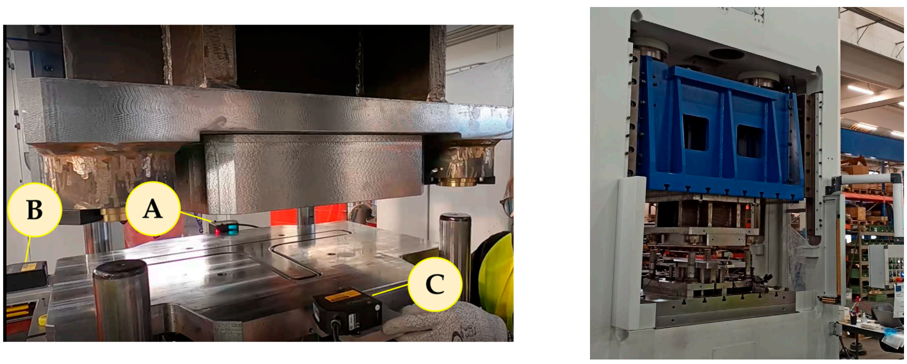

Figure 2. Hydraulic press machine adopted for experimental tests and laser triangulation sensors corresponding to the points (A, B and C) where the draw-in was monitored.

The calibrated FE model was adopted to evaluate the influence of the drawing depth (p) and the blank holder force (BHF) on the blank thinning (formability defect) and on the curvature of the part in the zone where the surface deflection occurs due to insufficient stretching (cosmetic defect). The thinning and the curvature were chosen as quality indices. After defining the acceptance limits for these indices, the values of the blank holder force and the drawing depth that respected these limits were identified as the design configuration. For this selected combination of BHF and p parameters, stochastic FE simulations were then performed by varying the friction coefficient (μ), yield strength (σ_0), ultimate tensile strength (σ_R), and mean anisotropy coefficient of the material (r_m), which were considered as noise parameters. It was evaluated how the noise parameters influence the two selected quality indices and the blank draw-in. This analysis was supported by metamodels obtained using the kriging technique. Metamodels allowed the detecting of the most sensitive sensor to the noise parameter variability and the noise parameter that most influenced the quality of the drawn component. Finally, based on the point-by-point difference between the draw-in in the design configuration and the one measured in the presence of a variation in the friction coefficient, a numerical control strategy was implemented using AutoForm and MATLAB R2022b software. Specifically, a closed-loop control was applied to the FE model so that variations in the blank holder force allowed for disturbance compensation. Using draw-in as trajectory tracking, blank holder force changes at each iteration, thanks to a proportional–integral–derivative (PID) controller, were modeled in MATLAB by means of the Ziegler–Nichols method.

2.1. FE Modeling

The FE model of the deep drawing process of the part in Figure 1 was developed by defining a blank in DC05 steel with a thickness of 0.75 mm and initial dimensions of 450 mm × 680 mm. DC05 steel was chosen since it is a cold-rolled low-carbon steel with excellent drawing and welding performance, widely adopted to manufacture various automotive parts [31]. The mechanical properties of this steel in terms of flow curve, yield surface, and forming limit curve (FLC), taken from the AutoformR10® library material database, are shown in Figure 3.

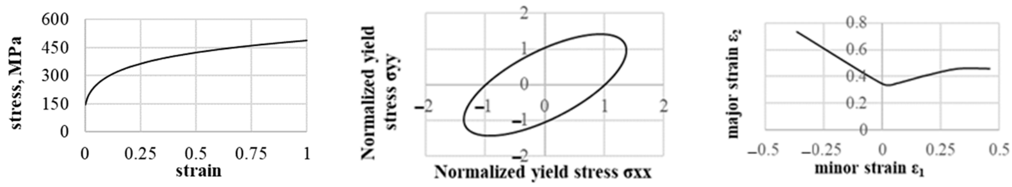

(**a**) (**b**) (**c**)

Figure 3. (**a**) Flow curve, (**b**) yield surface, and (**c**) FLC of DC05 steel.

The flow curve in Figure 3a is defined using a combination of the Swift and Hockett–Sherby approximation [32]. Equation (1) shows the expression for the calculation of flow stress. Table 1 collects all parameter values of the expression in Equation (1).

$$\sigma = (1-\alpha)\left\{C \times \left(\varepsilon_{pl} - \varepsilon_0\right)^m\right\} + \alpha\left(\sigma_{sat} - (\sigma_{sat} - \sigma_i)e^{-a\varepsilon_{pl}^{p}}\right) \quad (1)$$

Table 1. Parameters of Swift and Hockett–Sherby model.

Parameters	Value
α	0.25
C	515.5 MPa
ε_0	0.00607
σ_{sat}	413.1 MPa
σ_i	146.5 MPa
a	4.47

Yield surface in Figure 3b was defined according to the Hill48 model [33]. The yield surface according to the Hill model is assumed to be a quadratic function in stress space. The yield surface is defined using the three r values r_0, r_{45}, and r_{90} (plastic strain ratio with respect to 0°, 45°, and 90° of rolling direction) and the initial yield stress σ_0 in the rolling direction. Table 2 shows the values of Hill48 model parameters adopted in this study.

Table 2. Value of parameters of Hill48 model adopted for yield surface.

Parameters	Value
r_0	1.86
r_{45}	1.57
r_{90}	2.46
r_m	1.865
Biax	1

The parameter r_m represents the average value of the anisotropy and it is calculated as $r_m = (r_0 + 2r_{45} + r_{90})/4$. The Biax parameter is the biaxial stress factor, and it allows the yield surface to be expanded or contracted at the equi-biaxial stress points. This material-dependent value lies in the range from 0.8 to 1.2. If the biaxial stress factor is set equal to 1.0, then the classical Hill48 model is used.

The Arcelor V9 model was adopted to generate the FLC in Figure 3c. The uniform elongation ($A_{g,90}$) and the tensile strength along the 90° rolling direction were imposed, equal to 24.4% and 298.5 MPa, respectively.

The tools modeled in FE model are shown in Figure 4, from top to bottom: the punch, the blank holder and the die.

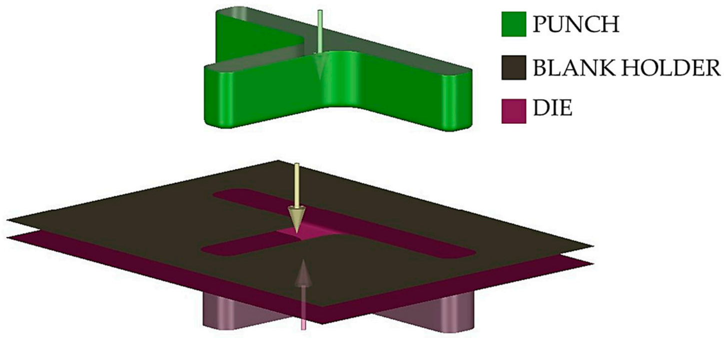

Figure 4. Punch, blank holder, and die modeled in FE model.

The die and the punch were taken as rigid bodies, and the blank holder was taken as a force-controlled tool. During the drawing process, the punch velocity was set equal to 8 mm/s.

Lubrication conditions were considered for the friction in the simulation. The Coulomb model with stick-slip modeling was used in the FE model. The friction coefficient applied was assumed between all tools and the blank. The friction coefficient value was calibrated based on the experimental data.

Once the FE model was developed, two sets of numerical simulations were performed.

The first one was designed to identify the influence of the drawing depth and the blank holder force on the quality of the drawn component. The parameters p and BHF were evaluated in the range of 25 mm–35 mm and 450 kN–950 kN, respectively. The quality of the drawn component was evaluated in terms of thinning and surface deflections. The first defect appeared prevalently at the angled parts of the component highlighted with T_A and T_B in Figure 5; the latter occurred in the central area of the component (region S_D in Figure 5). Thinning is a defect indicative of the material formability, and it indicates the change in thickness of the blank (relative to the original thickness) during the process. Surface deflections, on the other hand, are cosmetic defects, which are generally identified in the production process using the stoning technique [34] which can detect the out-of-plane geometric deviations and the difference between the ideal curve and the real one. In this work, these cosmetic defects were evaluated by means of a curvature analysis. The threshold values imposed on thinning and curvature so that a component without defects could be obtained were, respectively, 24% and 0.07 1/mm.

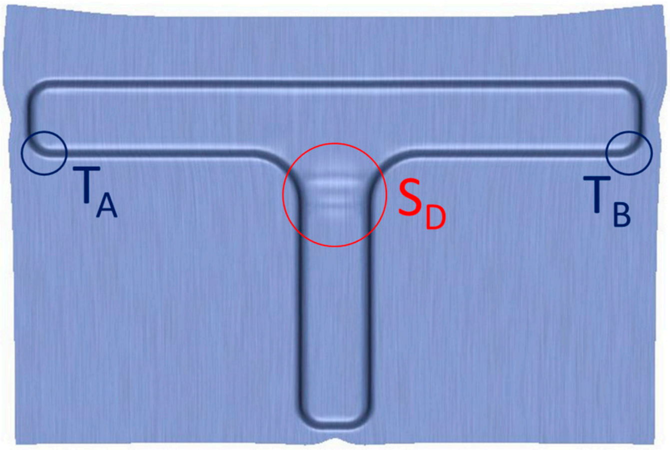

Figure 5. Areas of the component with formability and cosmetic defects (thinning in T_A and T_B and surface deflections in S_D).

At the end of this analysis, for a chosen combination of BHF and p which respect the limits on thinning and curvature (designed optimal configuration), another set of FE simulations was carried out. This second FE simulation set aimed to analyze the influence of the noise parameters (μ, σ_0, σ_R, r_m) both on the quality indexes and on the draw-in at the three points. The variability ranges of noise parameters are shown in Table 3 along with their nominal values.

Table 3. Noise parameters, nominal values, and variability ranges.

Noise Parameter	Nominal Value	Variability Range
σ_0, MPa	145.91	131.32–160.50
σ_R, MPa	285.50	256.96–314.06
r_m	1.86	1.49–2.23

During this analysis, the ratio between σ_0 and σ_R was kept constant and equal to 0.5.

The variation in r_m involves a variation in each single value of r_0, r_{90}, and r_{45}. Specifically, the new values of these latter parameters are proportional to the ratio between the new r_m value and the set nominal value. The mean value and the variability of the friction coefficient were defined after the calibration phase of the FE model.

All FE simulations were defined with elastic plastic shell elements and an initial element size of 20 mm with a maximum of 6 refinement levels and 11 layers through the thickness.

2.2. PID Modeling for Feedback Control on the Blank Holder Force

To obtain a component that complies with the quality limits, a feedback control based on the in-line draw-in measurement was modeled. This control was developed by combining the MATLAB and AutoForm tools. The former allowed us to model the PID controller, the latter to estimate the blank draw-in. Therefore, the FE software replaces the physical press machine. Figure 6 shows the block diagram of the process control. Specifically, the assumptions, that the drawing process was performed with a blank holder force equal to the optimal one (design condition) and the lubrication conditions between the tool and blank were changed (lower or higher friction coefficient), were adopted. For the new value of the friction coefficient, the FE simulation was performed with the aim of obtaining the blank draw-in (draw-in$_i$) in the new condition at the three monitored points. Based on the error (e), at each time step, between the draw-in value corresponding to the optimal blank holder force (draw-in$_{optimal}$) and the one measured (draw-in), the new value of the BHF able to minimize that error was calculated. The error value such that the control operates ($e_{accepted}$) was established based on preliminary FE simulations. The new BHF value was calculated using Equation (2).

$$BHF_i = BHF_{i-1} \pm \left(K_p e_i + K_d \frac{de_i}{dt} + K_i \int e_i \, dt \right) \tag{2}$$

where K_p, K_d, and K_i represent the PID gain factors. The contribution of the PID was added or subtracted from the initial BHF according to whether the measured draw-in was greater or less than the optimal one.

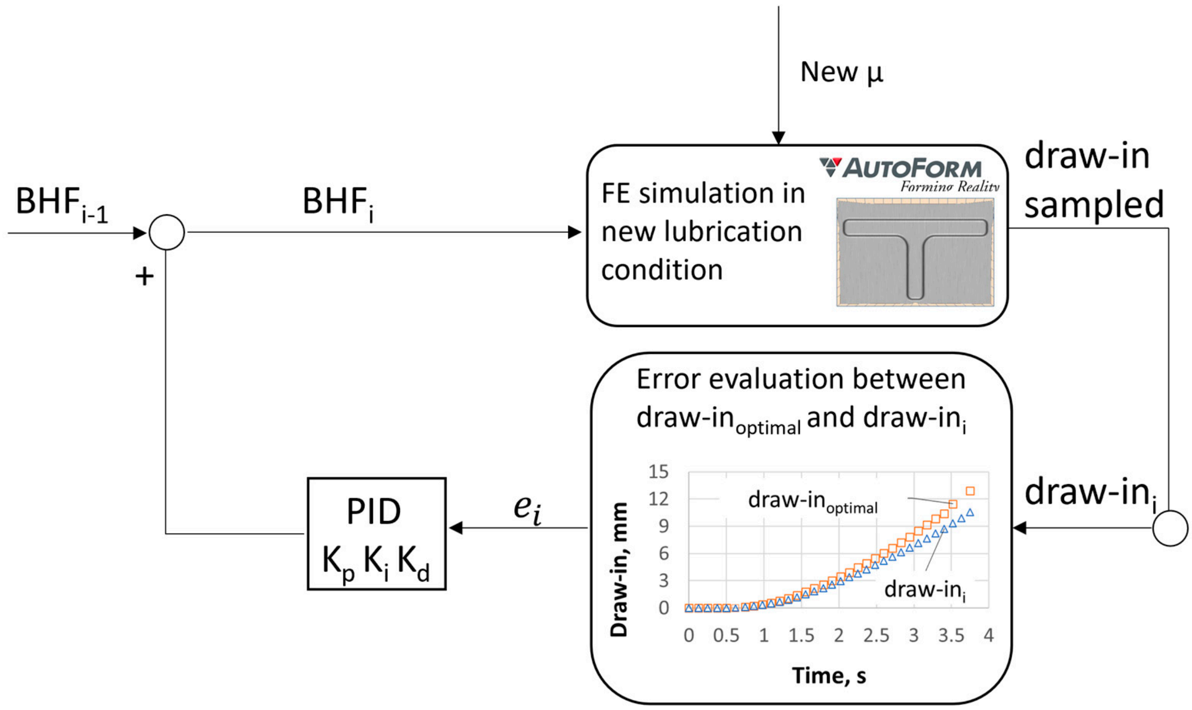

Figure 6. Block diagram of the feedback control.

The tuning method chosen in this study for identifying the values of the gain factors was the Ziegler–Nichols method [35]. This phase was supported by the Automated Ziegler–Nichols PID Tuning MATLAB code [36]. The identified values for K_p, K_i, and K_d were, respectively, 443.3, 0.39, and 0. Therefore, it is possible to state that a simple proportional–integrative (PI) control was adopted. The factor K_d was set equal to 0 since without the derivative term the system response was already stable. Several scientific studies adopted a simple PI controller for controlling stamping processes [37–42].

A saturator was implemented to limit the blank holder force at 1000 kN which is the maximum allowed force on the blank holder. It should be noted that during the step-by-step error calculation, the sensor that recorded a greater deviation from the optimal draw-in was monitored for the detection of the new BHF value.

3. Results

3.1. Calibration of FE Model by Means of Experimental Tests

Once the FE model was developed, preliminary numerical simulations allowed us to identify the variables that influence the process. In addition to the blank holder force and noise factors, i.e., the friction coefficient and material mechanical properties, the other variables that influence the process are the blank dimensions and positioning, kept constant in this study. During the experimental tests, the influence of all variables was limited. To this end, all initial blanks were laser-cut with the same dimensions (450 mm × 680 mm;

see Section 2.1), the blanks were always positioned in the same way respecting the initial distance from the laser sensors, the blanks were obtained from a single coil, and before each drawing operation lubricant oil was uniformly spread on the blanks.

However, to make the numerical simulation results consistent with the experimental ones, it was necessary to define the value of the friction coefficient to be set in the numerical model. This value was defined through the calibration phase, which involved choosing the value of the friction coefficient capable of minimizing the mean squared error between the experimentally measured draw-in and the numerically predicted one. Specifically, several numerical simulations were performed with different values of the friction coefficient. From the numerical results, the draw-in profile of the blank in the three points was obtained and these profiles were compared with the experimental ones. Finally, the value of the friction coefficient which guaranteed a lower mean squared error at each time step and for each of the three points was chosen.

The results of this phase led to a value of the friction coefficient equal to 0.11.

In Figure 7, the results in terms of the draw-in at points A, B, and C are shown for a blank holder force of 550 kN and a drawing depth of 30 mm. The experimental draw-in curves are shown with circular markers, while the numerical ones are shown with a solid line. A good agreement between the numerical and experimental draw-in results can be observed in Figure 7 for each sensor.

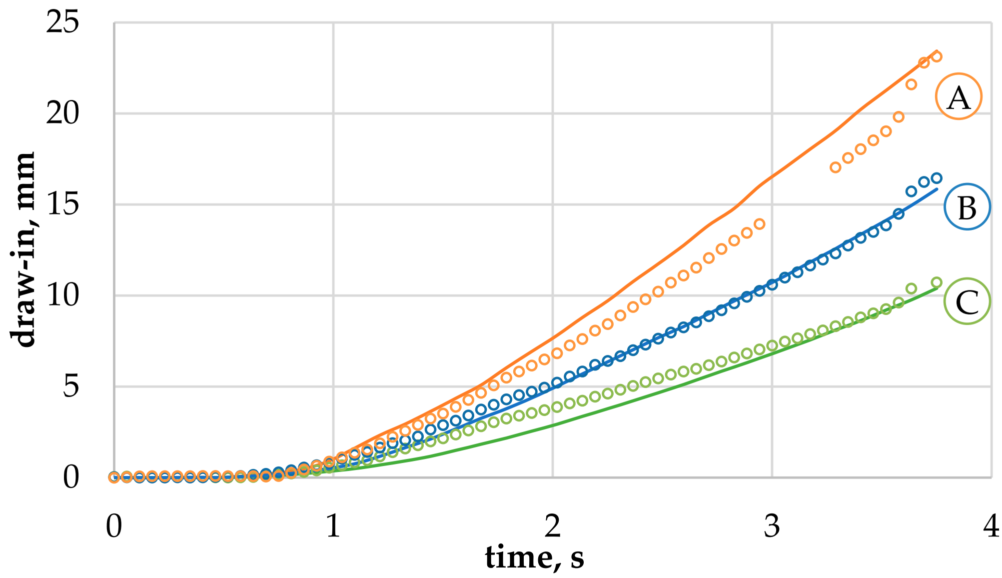

Figure 7. Comparison between experimental and numerical draw-in at points A, B, and C after calibration of FE model.

The numerical–experimental comparison in terms of the quality of the final drawn component is shown in Figure 8 for different values of blank holder force and drawing depth.

The qualitative comparison with the experimental results shows a good estimate of the numerical model, as it correctly predicts the area where surface cosmetic deflection occurs.

In Figure 8, on the FE-drawn part, the quantitative results in terms of curvature in the S_D region and thinning in the T_B region are also shown.

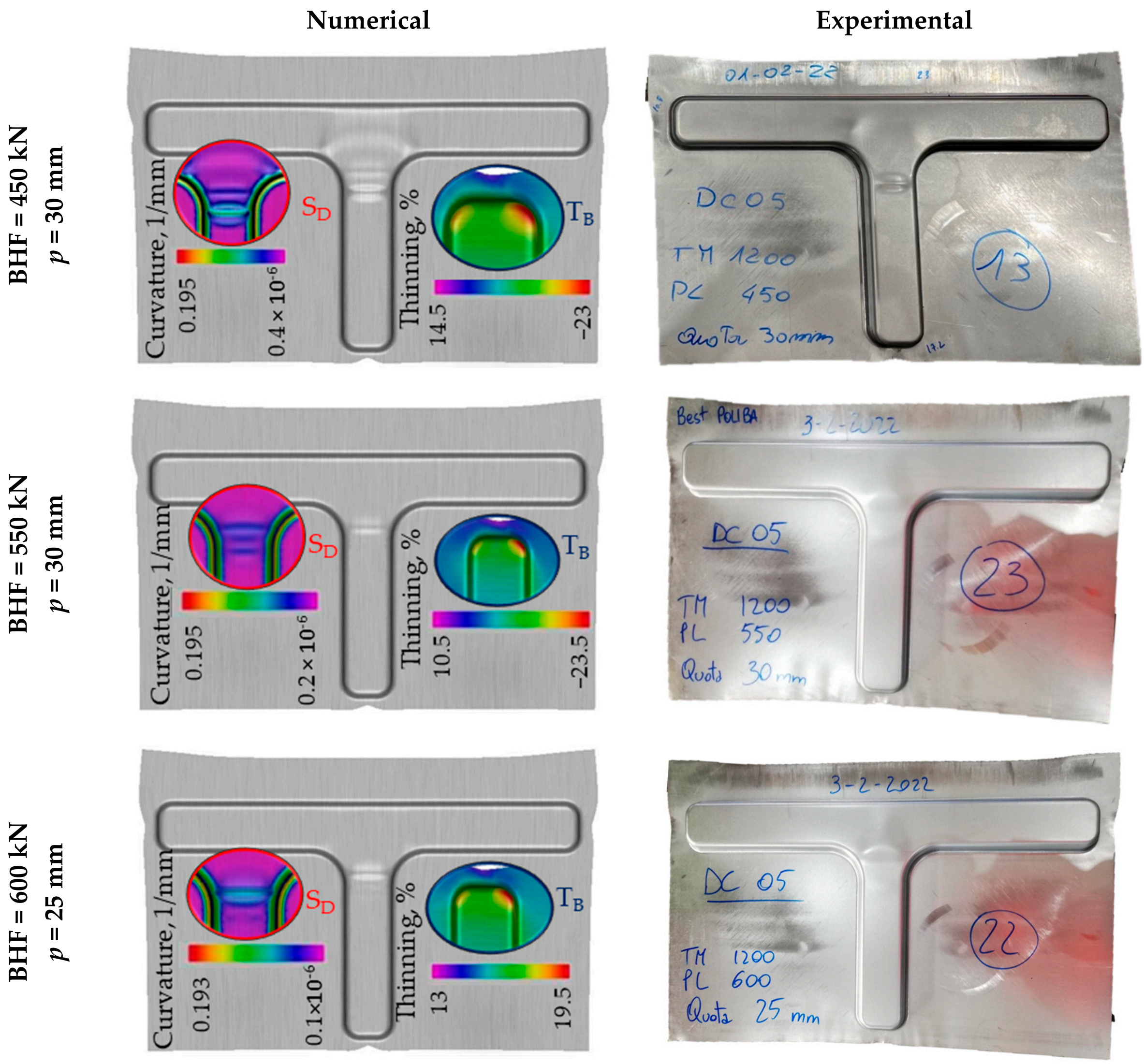

Figure 8. Numerical–experimental comparison of the drawn component for different values of BHF and *p*.

3.2. FE Analysis of BHF and p Parameters on the Quality of the Drawn Component

In Figure 9, for the case of BHF = 550 kN and p = 30 mm, the results of the thinning (Figure 9a) and curvature (Figure 9b) on the component are shown. The measure of the curvature is better emphasized by a view in the section A-A. The mean value of thinning in the region T_A is equal to that in the region T_B.

The results for each value of the blank holder force and the drawing depth are reported in Figure 10a for thinning and in Figure 10b for curvature.

From the graphs in Figure 10, it can be observed, as expected, that an increase in BHF leads to an increase in thinning but a reduction in the curvature. Moreover, an increase in p parameter causes an increase both in thinning and curvature.

These results are also confirmed by the graphs in Figure 11 which show, near the critical areas, the values of thinning (Figure 11a) and curvature (Figure 11b) as the parameters BHF and p vary. The combination of the parameters BHF and p such that the threshold values imposed for thinning and curvature are respected are shown in green. Conversely, the combinations of the parameters BHF and p that exceed the threshold values are shown in red. These figures can be adopted as a process window to choose the process parameter values to meet the required quality limits.

Based on these results, the analysis of the influence of noise parameters and the design of the control system were performed with a BHF equal to 650 kN and p equal to 30 mm. For this parameter pair, a thinning lower than 24% and a curvature lower than 0.07 1/mm are obtained in the corresponding critical regions of the part.

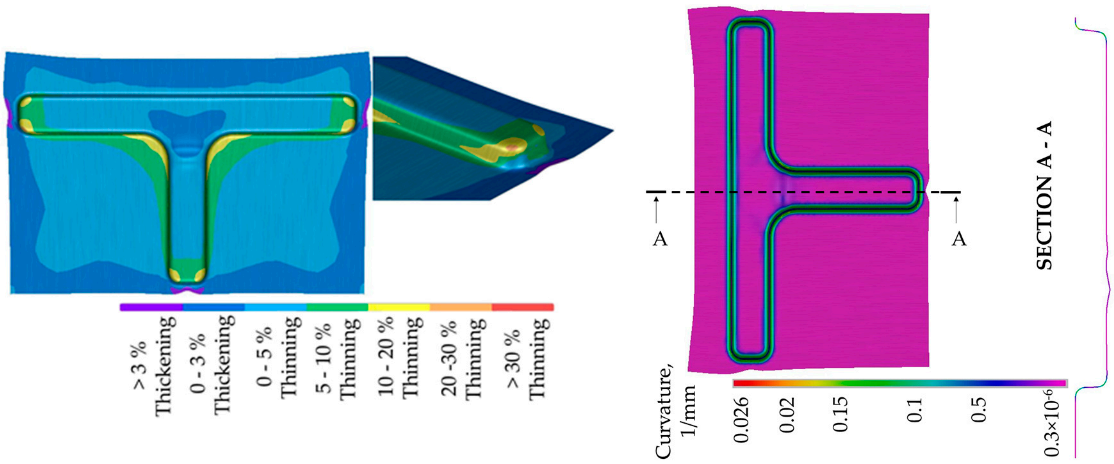

Figure 9. Results of (**a**) thinning and (**b**) curvature on the component.

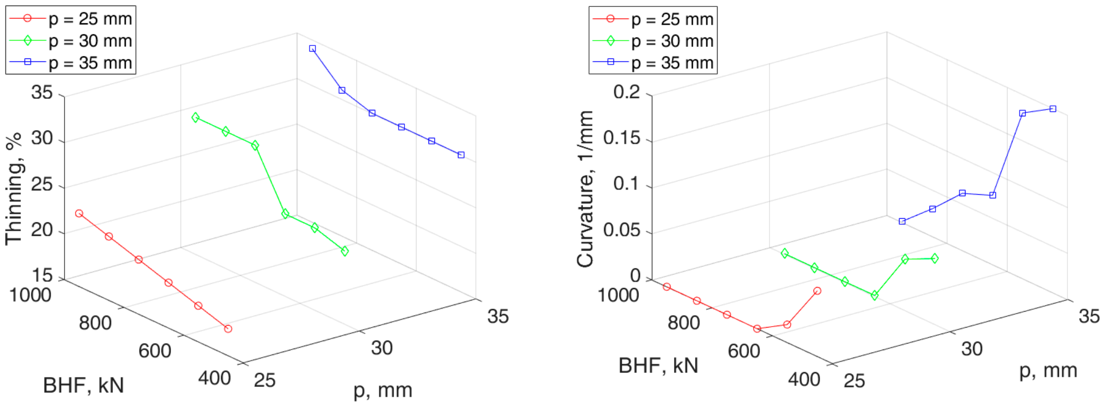

Figure 10. Influence of BHF and p on (**a**) thinning and (**b**) curvature.

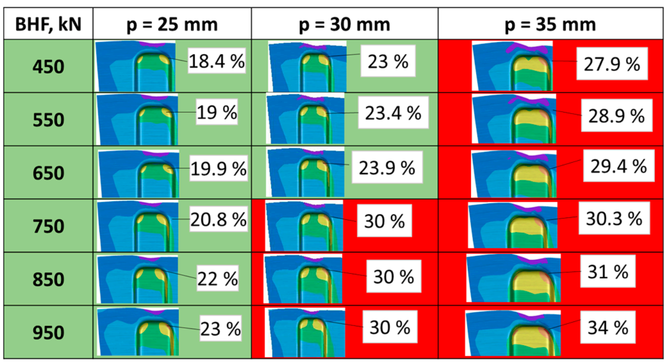

BHF, kN	p = 25 mm	p = 30 mm	p = 35 mm
450	18.4 %	23 %	27.9 %
550	19 %	23.4 %	28.9 %
650	19.9 %	23.9 %	29.4 %
750	20.8 %	30 %	30.3 %
850	22 %	30 %	31 %
950	23 %	30 %	34 %

(**a**)

Figure 11. *Cont.*

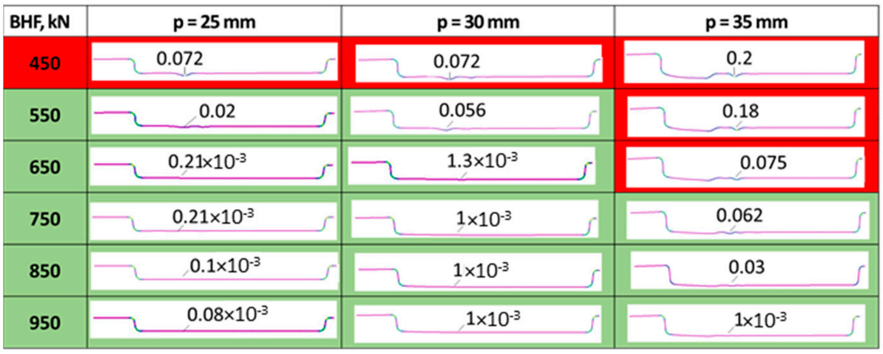

(**b**)

Figure 11. Graphical scheme of the combination of BHF and p parameters which assure/do not assure the threshold values for (**a**) thinning and (**b**) curvature.

3.3. Influence of Noise Parameters on the Quality of the Drawn Component

The influence of the noise parameter fluctuations on the quality of the drawn component was evaluated in terms of the thinning, surface deflections, and draw-in at points A, B, and C. The variability ranges of the noise parameters are shown in Table 3 along with their nominal values. For the friction coefficient, its nominal value was set equal to the experimentally calibrated one, i.e., 0.11, and a variability between 0.05 and 0.15 was imposed.

Sixty-three numerical simulations were performed by means of Latin Hypercube sampling. Data collected from FE simulations were processed by means of MATLAB DACE toolbox (2.0, Technical University of Denmark DK-2800 Kgs, Lyngby, Denmark) to derive metamodels with the kriging technique [43].

Metamodels highlighted in Figure 12 show the correlation between the thinning percentage and noise parameters such as μ and σ_0 (Figure 12a) and μ and r_m (Figure 12b). The other noise parameters are set to their nominal values (σ_R and r_m for the metamodel in Figure 12a, while σ_0 and σ_R for the metamodel in Figure 12b).

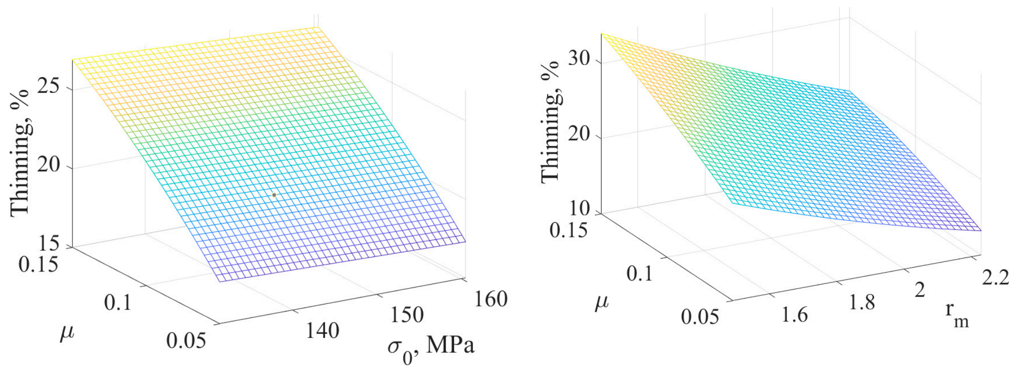

(**a**) (**b**)

Figure 12. Metamodel of thinning percentage for a fluctuation in (**a**) μ and σ_0 and (**b**) μ and r_m.

The results shown in Figure 12a highlight that σ_0 has little to no influence on thinning percentage, unlike μ, whose increasing values cause an increase in the thinning percentage. This thinning trend as a function of the friction coefficient is in agreement with the literature [10,44]. Figure 12b shows an increase in thinning percentage with a decrease in the mean anisotropy coefficient r_m. This behavior agrees with the literature [45].

Metamodels related to the curvature results are shown in Figure 13. Specifically, Figure 13a shows the curvature as a function of μ and σ_0 (σ_R and r_m set to the nominal values), while Figure 13b shows the curvature as a function of μ and r_m (σ_0 and σ_R set to nominal values). From the metamodel in Figure 13a, it is possible to observe a great influence of σ_0 on the curvature, which becomes even greater with increasing values of μ. The metamodel in Figure 13b shows that lower values of the friction coefficient result in a greater value of the curvature. This is due to the greater material flow with the reduction in the friction coefficient. Moreover, if the mean value of anisotropy has high values too, the curvature reaches its most critical levels.

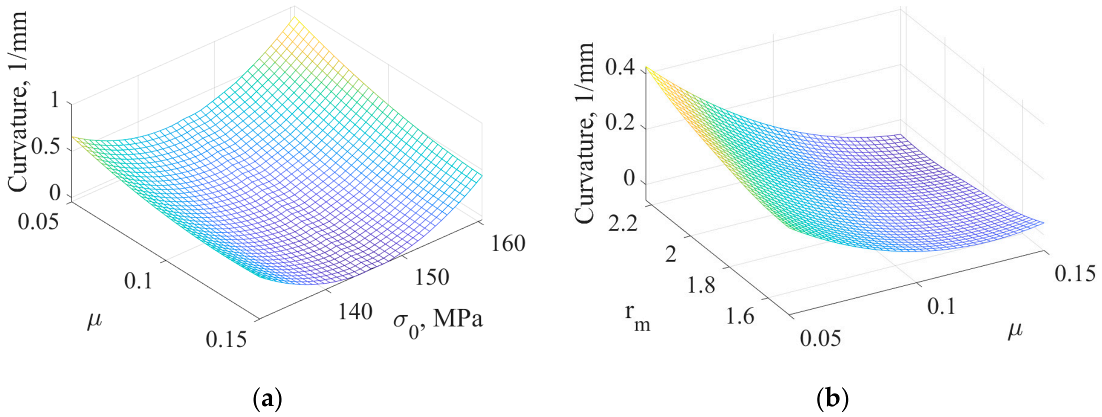

Figure 13. Metamodel of curvature for a fluctuation in (**a**) μ and σ_0 and (**b**) μ and r_m.

From the metamodels shown in Figures 12 and 13, it emerges that the most significant noise parameter for both quality indices is the friction coefficient. This result is confirmed by the variable dominating scatter analysis in AutoForm, which is an analysis that defines the most significant noise variable for the quality indexes and the regions where the noise variables exert the greatest influence. Figure 14 shows the obtained results.

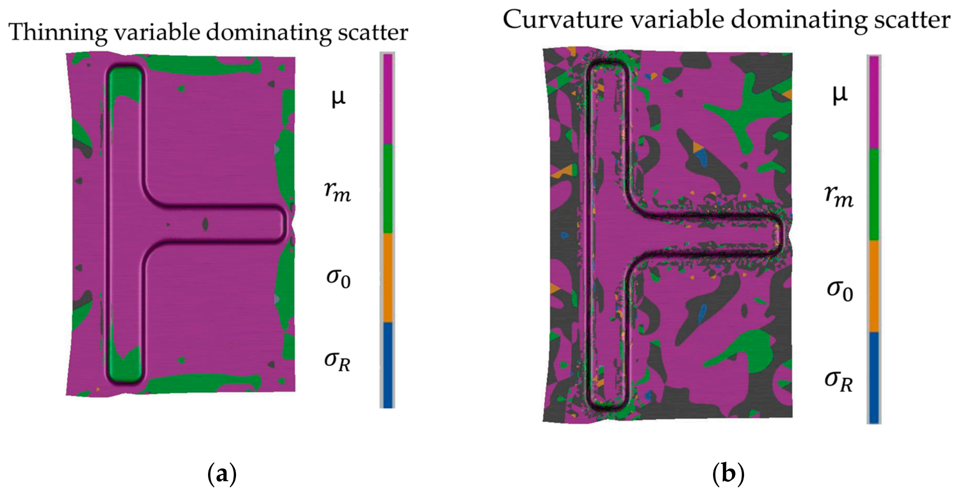

Figure 14. Noise parameter with the largest influence on the (**a**) thinning and (**b**) curvature.

Metamodels of the draw-in as a function of the noise parameters are illustrated in Figures 15–17, respectively, for sensors A, B, and C. From these figures, it is evident that for all three sensors, lower values of the friction coefficient increase the draw-in. While for the friction coefficient the relationship with the draw-in is quite linear and is the same for all three points considered, for the other two noise parameters this is not true. Specifically, the r_m coefficient has a low influence on the draw-in at sensors A and C (Figures 15b and 17b), whereas at sensor B higher values of it increase the draw-in (Figure 16b). As regards the σ_0 noise parameter, it has a low influence on the draw-in at sensor A (Figure 15a), whereas for sensor B the draw-in decreases for lower values of σ_0, but higher values of μ lead to a parabolic relationship between σ_0 and the draw-in (Figure 16a). The same behavior is observed for sensor C (Figure 17a).

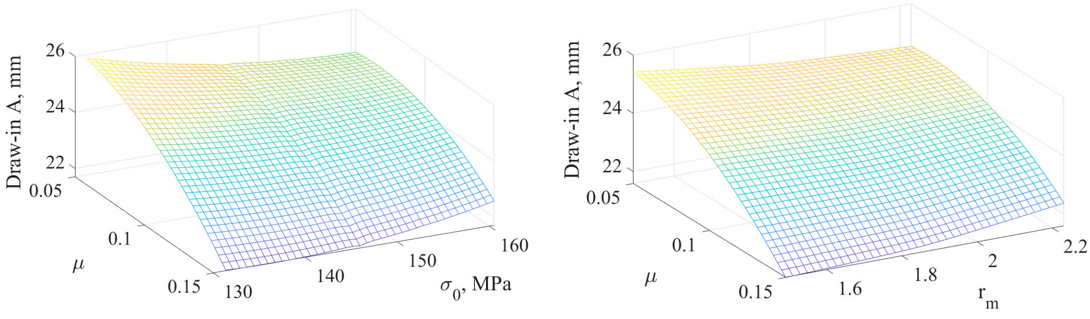

(**a**) (**b**)

Figure 15. Metamodel of the draw-in at point A for a fluctuation in (**a**) μ and σ_0 and (**b**) μ and r_m.

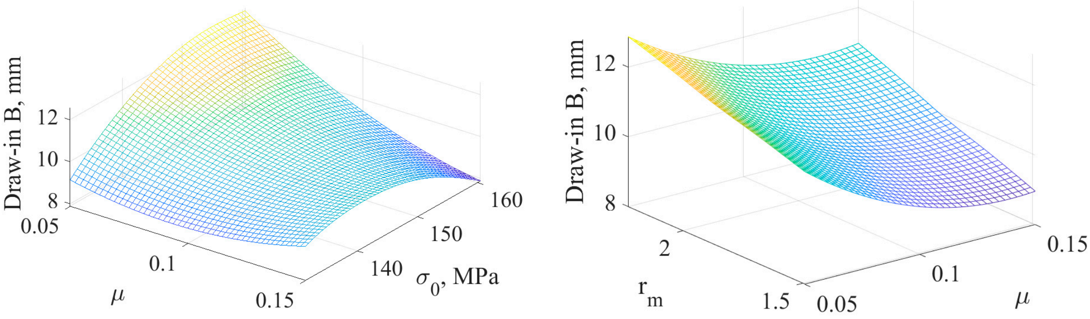

(**a**) (**b**)

Figure 16. Metamodel of the draw-in at point B for a fluctuation in (**a**) μ and σ_0 and (**b**) μ and r_m.

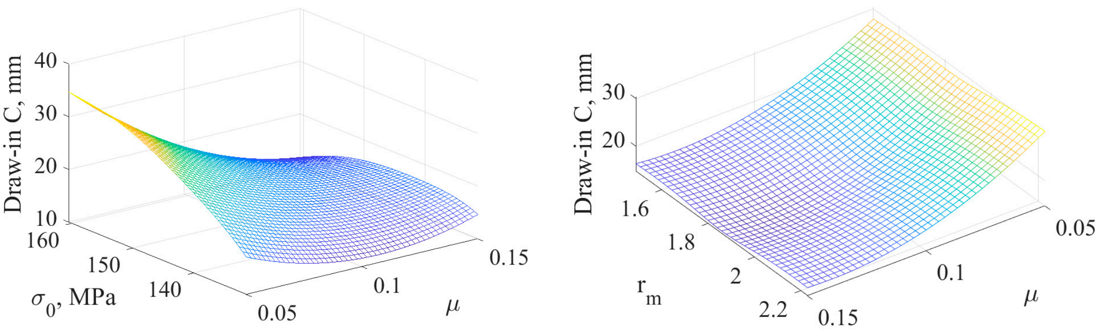

(**a**) (**b**)

Figure 17. Metamodel of the draw-in at point C for a fluctuation in (**a**) μ and σ_0 and (**b**) μ and r_m.

From these results, it can be stated that the relationships between the draw-in and the noise parameters σ_0 and r_m depend on the position considered for the blank, and so on the component shape. Furthermore, the sensor most sensitive to the variability in the noise factors is sensor C since the draw-in corresponding to this point changes from a minimum value of about 10 mm to a maximum value of about 30 mm. This is confirmed by the graphs in Figure 18 which shows, for each sensor, how the draw-in trajectory obtained with a friction coefficient equal to 0.11 (solid line) varies for the minimum value of the friction coefficient (0.05) and a maximum value (0.15). With respect to the value obtained with the calibrated friction coefficient (0.11), in the case of a friction coefficient equal to 0.05, the draw-in at the end of the deep drawing process corresponding to sensors A, B, and C increases by about 7%, 22%, and 141%, respectively. In the case of a friction coefficient of 0.15, the draw-in at the end of the deep drawing process at sensors A, B, and C is reduced by about 12%, 6%, and 11%, respectively.

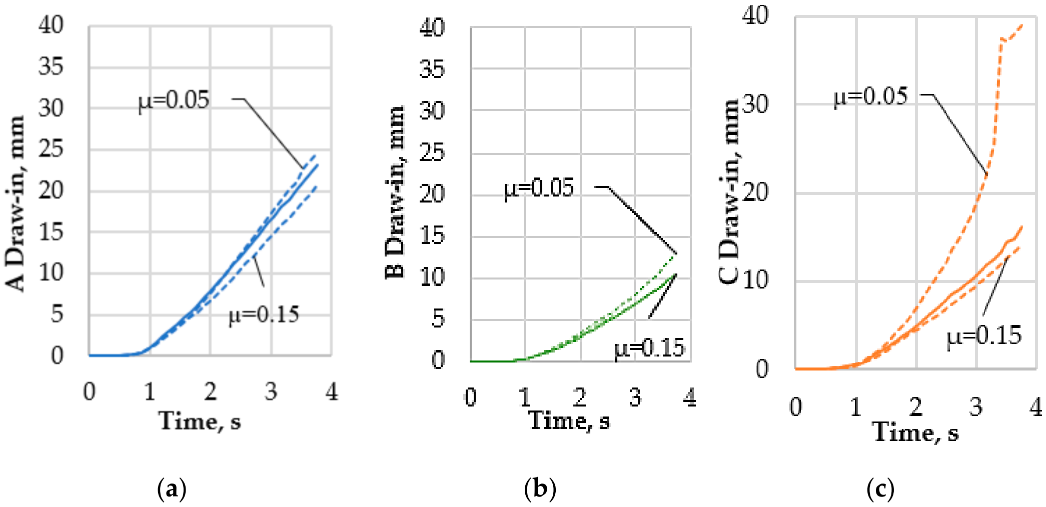

Figure 18. Draw-in over the time at point (**a**) A, (**b**) B, and (**c**) C for friction coefficient equal to 0.05, 0.11, and 0.15.

The greater variability in terms of draw-in is observed when the friction coefficient decreases. In that case, the sensor that appears to be more sensitive is sensor C. However, if the friction coefficient increases, the greater sensitivity is found for sensor A.

3.4. Feedback Control of the Draw-in by Regulating the BHF

The control methodology described in Section 2.2 was implemented by varying the friction coefficient in a range around the 0.11 value. Keeping the optimal blank holder force obtained for the 0.11 friction coefficient (650 kN), a friction reduction on the blank–tool interfaces shows surface deflections in the central region of the part (S_D region) due to the greater blank draw-in, as confirmed by observing the draw-in in sensors A, B, and C. With this assumption, the control system intervenes by increasing the force on the blank holder until it reaches the limit allowed by the press machine (1000 kN). The results obtained show that this limit condition is reached for a friction coefficient equal to 0.07. Conversely, an increase in the friction coefficient causes a decrease in the draw-in in each sensor and an increase in the split risk in the T_A and T_B regions. With a friction coefficient equal to 0.15, the thinning in these critical regions reaches 30%. Figure 19 summarizes the results obtained for a BHF equal to 650 kN and with the investigated friction condition limits (0.07, 0.15), comparing these results with those obtained for the optimized solution (μ0.11-650 kN). In the case of friction coefficients lower than 0.11, the maximum draw-in deviation occurs in sensor C, and the control system applies the feedback procedures on this sensor. For friction coefficients greater than 0.11, the control system applies the feedback procedures on sensor A because it is precisely in this sensor that the maximum draw-in deviations are recorded. Regarding the boundary friction condition investigated ($\mu = 0.07$ and $\mu = 0.15$), Figure 20 shows draw-in curves simulated in the controlled sensor and the blank holder force imposed to reduce draw-in deviations. In particular, the draw-in curves show the draw-in measured with a BHF equal to 650 kN (dashed curve), the draw-in taken as reference for deviation computation (continuous-line curve), and the draw-in measured following the blank holder force variations imposed by the control system (marked curve). These results have been obtained choosing a maximum draw-in deviation equal to 10% ($e_{accepted} = 0.1$). Furthermore, an adjustment time of the blank holder force of at least double compared to the response time of the hydraulic actuation (equal to 100 ms) was chosen.

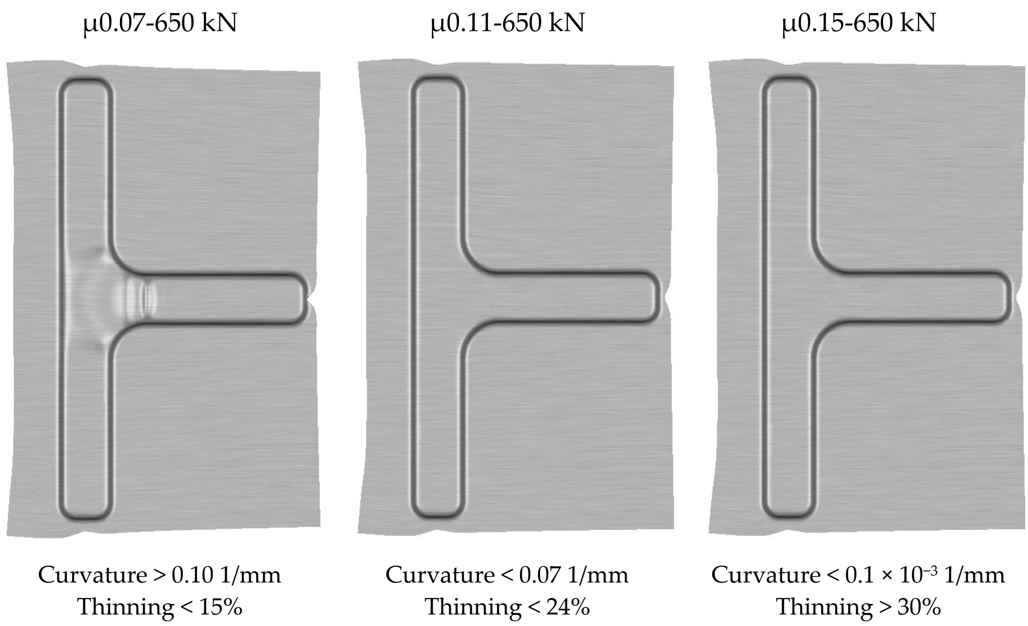

Figure 19. Formed parts' curvature and thinning values simulated with a BHF equal to 650 kN and different friction coefficients.

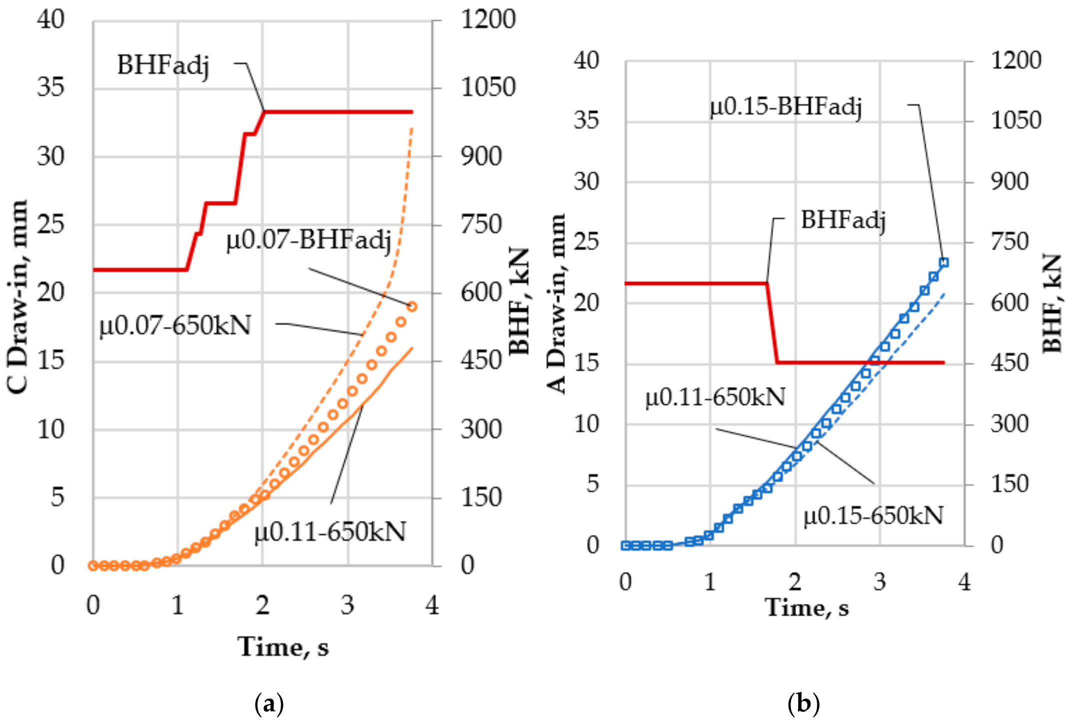

Figure 20. Draw-in curves and BHF adjusted in the controlled sensor with a friction coefficient equal to (**a**) 0.07 and (**b**) 0.15.

Assuming a friction coefficient equal to 0.07 (Figure 20a), the first sensor to have a draw-in deviation greater than $e_{accepted}$ is sensor C. To minimize the error between the draw-in measured in the optimal condition (μ0.11-650 kN) and that obtained for a friction coefficient equal to 0.07 (μ0.07-650 kN), the BHF was adjusted by increasing the force up to the 1000 kN limit value and then maintaining it constant (BHFadj). It is observed that, thanks to the BHF adjustment phase, the draw-in at C (μ0.07-BHFadj) approaches the optimal one, although the error obtained at the last time step is greater than 10% because the maximum admissible BHF was reached. The drawn component at the end of the process meets the quality requirements. Specifically, the curvature in region S_D is about 8.5×10^{-3} 1/mm, and the thinning percentage in regions T_A and T_B is equal to approximately 22%. The drawn part after BHF adjustment is like that obtained under the μ0.11-650 kN condition (Figure 19). Assuming a friction coefficient equal to 0.15 (Figure 20b), the first sensor to have a draw-in deviation greater than $e_{accepted}$ is sensor A. To minimize the error between the draw-in measured in the optimal condition (μ0.11-650 kN) and that obtained for a friction coefficient equal to 0.15 (μ0.15-650 kN), the BHF was adjusted by decreasing the force (BHFadj). It is observed that, thanks to the BHF adjustment phase, the draw-in at A (μ0.15-BHFadj) rapidly approaches the optimal one, and at the last time step the percentage error is about 1%. Thanks to the adjustment phase, the thinning in the T_A and T_B regions is no longer critical, as it is around 21%, while the curvature in the S_D region is about 0.01 1/mm.

After the adjustment phase, the uncontrolled sensors confirm the draw-in deviation reduction of the controlled sensor. Moreover, these draw-in deviations are always lower than $e_{accepted}$. Regarding a friction coefficient equal to 0.09, Figure 21 allows us to compare the draw-in adjusted curves simulated for each sensor (marked curves) with those obtained with a BHF equal to 650 kN (continuous-line curves). Sensor C remains the sensor that first shows an error greater than 10%, and a single change in the blank holder force (μ0.09-BHFadj curve) was required to reduce its draw-in deviation at the end of the process to around 4%. The BHF changes from 650 kN to 900 kN in about 200 ms. The draw-in curves of sensors A and B are also close to the optimal one. The T-shaped part obtained at the end of the adjusted deep drawing process is like that obtained under the μ0.11-650 kN condition (Figure 19), while thinning in the T_A and T_B regions is around 21% and the curvature in the S_D region is around 1.2×10^{-3} 1/m.

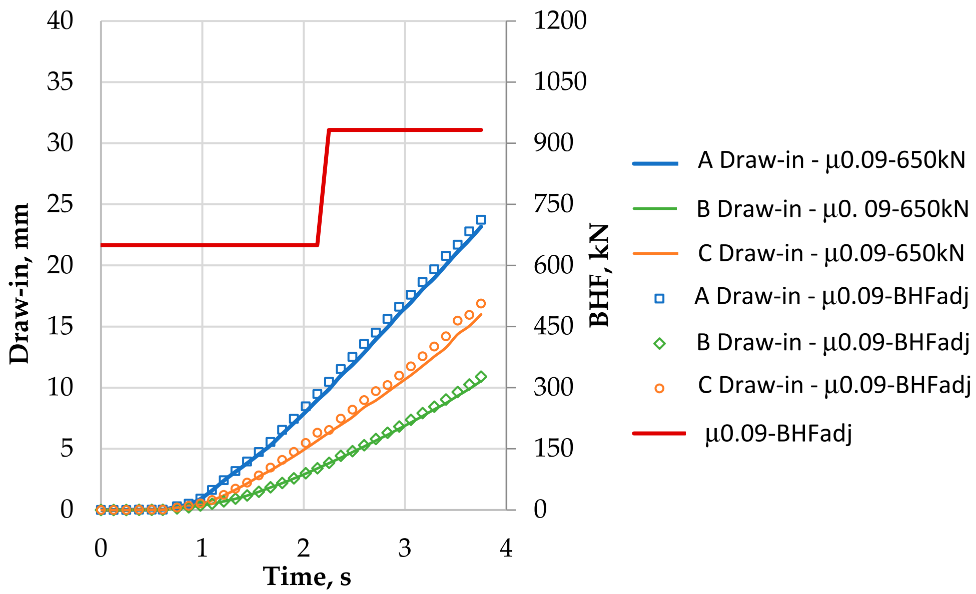

Figure 21. Results after BHF adjustment for μ = 0.09 in terms of draw-in and BHF adjustment curve.

4. Conclusions

The case study presented here allowed us to study how formability defects, i.e., thinning, and cosmetic defects, i.e., surface deflections, are influenced by process and noise parameters. These typical defects of the deep drawing process can be measured only in the post-forming phase. After the forming phase, if the component does not meet the quality indexes due to the scattering in material properties or in lubrication conditions during the process, it becomes a production waste. For this reason, this case study was also adopted to implement a numerical procedure to adjust in-line the BHF based on the in-line measurement of the blank draw-in. The goal is the obtaining of a drawn component that satisfies the quality limits even in the presence of scattering in noise parameters, thus reducing production waste.

The FE results demonstrated that the most significant noise factor is the friction coefficient. Its reduction leads to a greater blank draw-in, worsening the surface deflections on the component. Conversely, an increase in the friction coefficient leads to a reduction in the blank draw-in, which in turn increases the risk of splits.

The implemented regulation methodology is able to increase or decrease the blank holder force depending on whether the blank sliding is greater or lower than that recorded in optimal conditions.

The results for the case study show that:

- Checking only the sensor that highlights the greatest deviation in the draw-in from the optimal one allows us to obtain a drawn component that falls within the imposed quality limits. After BHF adjustment, the percentage error between the measured draw-in and the optimal one decreases. This is observed both in the controlled and uncontrolled sensors.
- When the percentage error between the measured draw-in and the optimal one is high, the BHF adjustment becomes more difficult since more control steps are required to minimize the error. Therefore, a combination of the feedback control type and feed-forward control type will be required to estimate the friction coefficient value and identify the new optimal BHF.

Author Contributions: Conceptualization, L.T. and M.E.P.; methodology, L.T. and M.E.P.; software, M.E.P.; validation, M.E.P.; formal analysis, M.E.P.; investigation, M.E.P.; resources, L.T.; data curation, M.E.P.; writing—original draft preparation, M.E.P.; writing—review and editing, L.T. and M.E.P.; visualization, L.T. and M.E.P.; supervision, L.T.; project administration, L.T.; funding acquisition, L.T. All authors have read and agreed to the published version of the manuscript.

Funding: This research was funded by the PNRR—Spoke 11 (Innovative Materials and Lightweighting) project—CUP-D93C22000410001 and PICO&PRO project—COD.ID.ARS01_01061.

Institutional Review Board Statement: Not applicable.

Informed Consent Statement: Not applicable.

Data Availability Statement: Not applicable.

Acknowledgments: The authors are grateful to AutoForm Engineering GmbH for the support in FE model development and to partners of the PICO & PRO project. The authors also thank the engineers Elena Fiermonte and Andrea Nono Dachille for the support in the finite element simulations.

Conflicts of Interest: The authors declare no conflict of interest.

References

1. Kraft, M.; Bürgel, U. Novel concept for measurement of global blank draw-in when deep drawing outer skin automotive components. *J. Phys. Conf. Ser.* **2017**, *896*, 012034. [CrossRef]
2. Swapna, D.; Srinivasa Rao, C.; Radhika, S. A review on deep drawing process. *Int. J. Emerg. Res. Manag. Technol.* **2018**, *6*, 146–149. [CrossRef]
3. Dal Santo, P.; Germain, G.; Boude, S.; Giraud, E. Cold forming by stretching of aeronautic sheet metal parts. *Int. J. Comput. Integr. Manuf.* **2014**, *27*, 129–138. [CrossRef]
4. Zein, H.; El-Sherbiny, M.; Abd-Rabou, M.; El Shazly, M. Effect of die design parameters on thinning of sheet metal in the deep drawing process. *Am. J. Mech. Eng.* **2013**, *1*, 20–29. [CrossRef]
5. Zhang, H.; Qin, S.; Cao, L. Investigation of the effect of blank holder force distribution on deep drawing using developed blank holder divided into double rings. *J. Braz. Soc. Mech. Sci. Eng.* **2021**, *43*, 284. [CrossRef]
6. Krishnan, N.; Cao, J. Estimation of optimal blank holder force trajectories in segmented binders using an ARMA model. *J. Manuf. Sci. Eng.* **2003**, *125*, 763–770. [CrossRef]
7. Ahmetoglu, M.A.; Coremans, A.; Kinzel, G.L.; Altan, T. *Improving Drawability by Using Variable Blank Holder Force and Pressure in Deep Drawing of Round and Non-Symmetric Parts*; No. 930287; SAE Technical Paper; SAE International: Warrendale, PA, USA, 1993.
8. Palmieri, M.; Lorusso, V.; Tricarico, L. Robust optimization and Kriging metamodeling of deep-drawing process to obtain a regulation curve of blank holder force. *Metals* **2021**, *11*, 319. [CrossRef]
9. E Palmieri, M.; Tricarico, L. Control of draw-in in the deep-drawing process by regulating the force on the blank holder. *IOP Conf. Ser. Mater. Sci. Eng.* **2022**, *1238*, 012071. [CrossRef]

10. Atul, S.T.; Babu, M.L. A review on effect of thinning, wrinkling and spring-back on deep drawing process. *Proc. Inst. Mech. Eng. Part B J. Eng. Manuf.* **2019**, *233*, 1011–1036. [CrossRef]
11. Wiebenga, J.; Atzema, E.; An, Y.; Vegter, H.; Boogaard, A.V.D. Effect of material scatter on the plastic behavior and stretchability in sheet metal forming. *J. Mater. Process. Technol.* **2014**, *214*, 238–252. [CrossRef]
12. Fischer, P.; Harsch, D.; Heingärtner, J.; Renkci, Y.; Hora, P. Inline feedback control for deep drawing applications. *IOP Conf. Ser. Mater. Sci. Eng.* **2016**, *159*, 012006. [CrossRef]
13. Merten, M.; Liebold, K.; Haufe, A. Robustness analysis with LS-OPT®and LS-DYNA®for sheet metal forming simulations. *IOP Conf. Ser. Mater. Sci. Eng.* **2021**, *1157*, 012088. [CrossRef]
14. Wiebenga, J.H. Robust Design and Optimization of Forming Processes. Ph.D. thesis, University of Twente Faculty of Engineering Technology, Enschede, The Netherlands, 2014.
15. Kim, K.; Jeong, J.Y.; Yong, S.S. Process optimization of sheet metal forming using operating window. *Int. Des. Eng. Tech. Conf. Comput. Inf. Eng. Conf.* **2009**, *49057*, 209–216.
16. Fischer, P.; Heingärtner, J.; Renkci, Y.; Hora, P. Experiences with inline feedback control and data acquisition in deep drawing. *Procedia Manuf.* **2018**, *15*, 949–954. [CrossRef]
17. Fischer, P.; Harsch, D.; Heingärtner, J.; Renkci, Y.; Hora, P. Implementation of feedback control in kitchen sink production. *IOP Conf. Ser. Mater. Sci. Eng.* **2018**, *418*, 012110. [CrossRef]
18. Fischer, P.; Harsch, D.; Heingärtner, J.; Renkci, Y.; Hora, P. A knowledge-based control system for the robust manufacturing of deep drawn parts. *Procedia Eng.* **2017**, *207*, 42–47. [CrossRef]
19. Available online: https://ahssinsights.org/news/vision-for-industry-4-0-in-sheet-metal-forming/ (accessed on 10 December 2022).
20. Hardt, D.E.; Fenn, R.C. Real-time control of sheet stability during forming. *J. Eng. Ind.* **1993**, *115*, 299–308. [CrossRef]
21. Endelt, B.; Nielsen, K.B.; Danckert, J. New framework for on-line feedback control of a deep-drawing operation. *J. Mater. Process. Technol.* **2006**, *177*, 426–429. [CrossRef]
22. Endelt, B.; Tommerup, S.; Danckert, J. A novel feedback control system–Controlling the material flow in deep drawing using distributed blank-holder force. *J. Mater. Process. Technol.* **2013**, *213*, 36–50. [CrossRef]
23. Lo, S.W.; Jeng, G.M. Monitoring the displacement of a blank in a deep drawing process by using a new embedded-type sensor. *Int. J. Adv. Manuf. Technol.* **1999**, *15*, 815–821. [CrossRef]
24. Doege, E.; Seidel, H.-J.; Griesbach, B.; Yun, J.-W. Contactless on-line measurement of material flow for closed loop control of deep drawing. *J. Mater. Process. Technol.* **2002**, *130*, 95–99. [CrossRef]
25. Doege, E.; Schmidt-Jürgensen, R.; Huinink, S.; Yun, J.-W. Development of an optical sensor for the measurement of the material flow in deep drawing processes. *CIRP Ann.* **2003**, *52*, 225–228. [CrossRef]
26. Mahayotsanun, N.; Cao, J.; Peshkin, M. A Draw-In Sensor for Process Control and Optimization. *AIP Conf. Proc.* **2005**, *778*, 861–866.
27. Kott, M.; Erz, C.; Heingärtner, J.; Groche, P. Controllability of Temperature Induced Friction Effects during Deep Drawing of Car Body Parts with High Drawing Depths in Series Production. *Procedia Manuf.* **2020**, *47*, 553–560. [CrossRef]
28. Bäume, T.; Zorn, W.; Drossel, W.G.; Rupp, G. Iterative process control and sensor evaluation for deep drawing tools with integrated piezoelectric actuators. *Manuf. Rev.* **2016**, *3*, 3. [CrossRef]
29. Bäume, T.; Zorn, W.; Drossel, W.-G.; Rupp, G. Step by step control of a deep drawing process with piezo-electric actuators in serial operation. *MATEC Web Conf.* **2015**, *21*, 04008. [CrossRef]
30. Brun, M.; Ghiotti, A.; Bruschi, S.; Filippi, S. Active control of blankholder in sheet metal stamping. *Procedia CIRP* **2021**, *100*, 151–156. [CrossRef]
31. Available online: https://www.esb-group.com/en/products-din-en/cold-rolled-steel/ (accessed on 29 November 2022).
32. Banabic, D.; Sester, M. Influence of material models on the accuracy of the sheet forming simulation. *Mater. Manuf. Process.* **2012**, *27*, 273–277. [CrossRef]
33. Hill, R. A theory of the yielding and plastic flow of anisotropic metals. *Proc. R. Soc. Lond. Ser. A Math. Phys. Sci.* **1948**, *193*, 281–297.
34. Shen, H.; Li, S.; Chen, G. Quantitative analysis of surface deflections in the automobile exterior panel based on a curvature-deviation method. *J. Mater. Process. Technol.* **2012**, *212*, 1548–1556. [CrossRef]
35. Ziegler, J.G.; Nichols, N.B. Optimum settings for automatic controllers. *Trans. ASME* **1942**, *64*, 759–765. [CrossRef]
36. Waleed, E.-B. Automated Ziegler Nicholas PID Tuning. MATLAB Central File Exchange. Available online: https://www.mathworks.com/matlabcentral/fileexchange/47836-automated-ziegler-nicholas-pid-tuning (accessed on 19 December 2022).
37. Cao, J.; Boyce, M.C. Design and control of forming parameters using finite element analysis. *Am. Soc. Mech. Eng. Aerosp. Div. (Publ.) AD* **1994**, *42*, 265–285.
38. Sunseri, M.; Cao, J.; Karafillis, A.P.; Boyce, M.C. Accommodation of springback error in channel forming using active binder force control: Numerical simulations and experiments. *J. Eng. Mater. Technol.* **1996**, *118*, 426–435. [CrossRef]
39. Siegert, K.; Ziegler, M.; Wagner, S. Closed loop control of the friction force. Deep drawing process. *J. Mater. Process. Technol.* **1997**, *71*, 126–133. [CrossRef]
40. Ziegler, M. *Pulsating Blankholder Technology*; No. 1999-01-3155; SAE Technical Paper; SAE International: Warrendale, PA, USA, 1999.

41. Hsu, C.-W.; Ulsoy, A.G.; Demeri, M.Y. Development of process control in sheet metal forming. *J. Mater. Process. Technol.* **2002**, *127*, 361–368. [CrossRef]
42. Lim, Y. MIMO Adaptive Process Control in Stamping Using Punch Force. Ph.D. Thesis, University of Michigan, Ann Arbor, MI, USA, 2010.
43. Kleijnen, J.P.C. Kriging metamodeling in simulation: A review. *Eur. J. Oper. Res.* **2009**, *192*, 707–716. [CrossRef]
44. Zein, H.; El Sherbiny, M.; Abd-Rabou, M.; El Shazly, M. Thinning and spring back prediction of sheet metal in the deep drawing process. *Mater. Des.* **2014**, *53*, 797–808. [CrossRef]
45. Bhaduri, A. *Deep Drawing. Mechanical Properties and Working of Metals and Alloys*; Springer: Singapore, 2018; pp. 693–719.